Nano Energy 27 (2016) 27–34

Contents lists available at ScienceDirect

Nano Energy

journal homepage: www.elsevier.com/locate/nanoen

Layered P2-$Na_{2/3}[Ni_{1/3}Mn_{2/3}]O_2$ as high-voltage cathode for sodium-ion batteries: The capacity decay mechanism and Al_2O_3 surface modification

Yihang Liu [a,1], Xin Fang [b,1], Anyi Zhang [b], Chenfei Shen [b], Qingzhou Liu [b], Hani A. Enaya [c,d], Chongwu Zhou [a,*]

[a] Department of Electrical Engineering, University of Southern California, Los Angeles, CA 90089, United States
[b] Department of Chemical Engineering and Material Science, University of Southern California, Los Angeles, CA 90089, United States
[c] King Abdulaziz City for Science and Technology, Riyadh, Saudi Arabia
[d] Department of Electrical Engineering, University of California at Los Angeles, Los Angeles, CA 90095, United States

ARTICLE INFO

Article history:
Received 18 February 2016
Received in revised form
15 June 2016
Accepted 16 June 2016
Available online 17 June 2016

Keywords:
Sodium-ion batteries
High voltage cathode
Surface coating
Exfoliation
P2-$Na_{2/3}[Ni_{1/3}Mn_{2/3}]O_2$
Layered metal oxide cathode

ABSTRACT

The P2 type $Na_{2/3}[Ni_{1/3}Mn_{2/3}]O_2$ is a high-voltage cathode material for Na-ion batteries with a theoretical capacity of 173 mA h/g and a long operation voltage plateau of 4.2 V. However, the material has exhibited unstable cycling performance within the high-voltage window, which severely limits its application. Moreover, its capacity decay mechanism is still unclear. In this study, we first investigate the difference between as-prepared and after-cycling $Na_{2/3}[Ni_{1/3}Mn_{2/3}]O_2$ samples, and then confirmed that the transition metal oxide layer exfoliation associated with the crystal phase transition during Na ion extraction and insertion is the main cause of capacity fading. The Al_2O_3 coated $Na_{2/3}[Ni_{1/3}Mn_{2/3}]O_2$ with enhanced cycling performance was prepared by taking the benefit of Al_2O_3 coating. The $Na_{2/3}[Ni_{1/3}Mn_{2/3}]O_2$ sample without any surface modification presented a 164 mA h/g initial specific discharge capacity within the voltage window from 2.5 V to 4.3 V, and the capacity decayed to 44 mA h/g at the 300th cycle, resulting in only a 26.8% retention. In contrast, the Al_2O_3-coated $Na_{2/3}[Ni_{1/3}Mn_{2/3}]O_2$ presented a similar initial capacity, but with an enhanced 73.2% retention after 300 cycles. The enhanced cycling stability observed in after-cycling characterization and analysis confirms that the Al_2O_3 surface coating can effectively suppress the unfavorable side reaction at high voltage and the exfoliation of the metal oxide layers.

1. Introduction

Na-ion batteries potentially offer a lower cost, safer and more environmentally friendly battery system than Li-ion batteries [1,2]. Several promising cathode materials with high energy density and cycling stability have been developed, such as phosphates/fluorophosphates and Prussian blue type materials [3–9]. However, Li-ion battery still dominates the power supplies of the electric vehicles and portable devices because of its high energy density and excellent cycling stability [10]. Layered structure materials, such as P2-type and O3-type materials, have been extensively studied and are considered one of the most promising cathode material candidates for next generation Na-ion batteries [11–16]. Similar to $Li[Ni_{0.5}Mn_{1.5}]O_4$, P2-type $Na_{2/3}[Ni_{1/3}Mn_{2/3}]O_2$ can serve as a sodium insertion host at high operating voltages, since all the Na ions can be reversibly extracted based on the Ni^{2+}/Ni^{4+} redox [17,18]. Achieving reversible Na ion extraction at high operating voltages is highly beneficial to increase the energy density of Na-ion cathodes. However, the P2-O2 crystal phase transition and the large volume change of the O2 phase (more than 20%) is unavoidable since the O2 structure has a lower formation energy density than the P2 structure at high voltages [19,20]. This severely damages the cycling stability within the high voltage window. As a result, the $Na_{2/3-x}[Ni_{1/3}Mn_{2/3}]O_2$ can only obtain stable electrochemical performance in the region of $0 \le x \le 1/3$, which greatly limits the energy and power density of $Na_{2/3}[Ni_{1/3}Mn_{2/3}]O_2$ for real applications. In order to achieve sufficiently good cyclability, several attempts were reported such as the substitution of transition metal ions and lithium ions [21,22]. Despite these substitutions, the stable cycling performance has still been limited to ~100 cycles due to an unclear capacity decay mechanism.

In this study, we first explored the electrochemical performance and capacity decay mechanism of $Na_{2/3}[Ni_{1/3}Mn_{2/3}]O_2$ within a high voltage window from 2.5 V to 4.3 V. Based on the discovered degradation mechanism, we applied a surface-coating

* Corresponding author.
E-mail address: chongwuz@usc.edu (C. Zhou).
[1] These authors contributed equally.

http://dx.doi.org/10.1016/j.nanoen.2016.06.026
2211-2855/

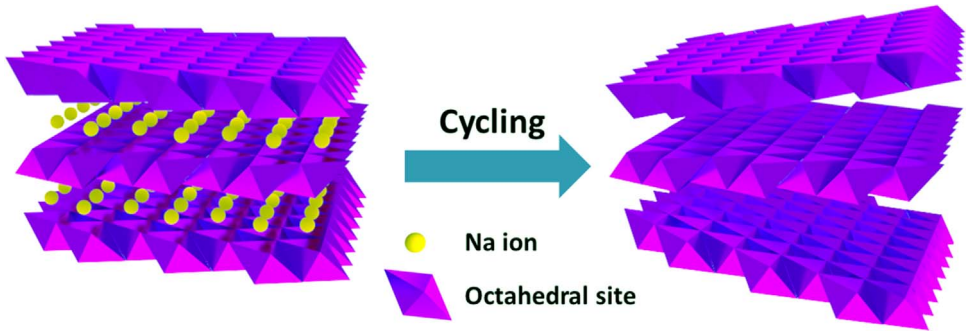

Fig. 1. Schematic figure of the exfoliation during the sodiation and de-sodiation process of the P2-$Na_{2/3}[Ni_{1/3}Mn_{2/3}]O_2$ particle.

solution to stabilize the $Na_{2/3}[Ni_{1/3}Mn_{2/3}]O_2$ electrode using a simple wet chemistry method. As illustrated schematically in Fig. 1 (a), the exfoliation phenomena resulting from an unfavorable crystal structure transition was observed in the after-cycling $Na_{2/3}[Ni_{1/3}Mn_{2/3}]O_2$ particles. Furthermore, an Al_2O_3 surface coating was applied on $Na_{2/3}[Ni_{1/3}Mn_{2/3}]O_2$ particles (Al_2O_3-$Na_{2/3}[Ni_{1/3}Mn_{2/3}]O_2$) and effectively solved the issues discussed above and enhanced the cycling life. We employed an Al_2O_3 coating because Al_2O_3 been shown to be an excellent coating material for mitigating volume expansion and contraction during Li/Na ion insertion and extraction [23–26]. Because P2-$Na_{2/3}[Ni_{1/3}Mn_{2/3}]O_2$ is stable in moist air and, it is compatible with wet chemistry surface coating or other surface modification methods involving water [27]. The comparison between the fresh and cycled electrodes together with the enhanced cycling performance by robust Al_2O_3 coating revealed the mechanism of capacity decay, and further demonstrated that the Al_2O_3 surface coating can suppress the side reaction and protect the layered metal oxide particles during long cycling within the high voltage window. The designed Al_2O_3-$Na_{2/3}[Ni_{1/3}Mn_{2/3}]O_2$ cathode is ideal for large scale high power/energy Na-ion storage, not only because of its excellent cycling stability and improved voltage profile, but also due to the scalability of the solid state reaction of $Na_{2/3}[Ni_{1/3}Mn_{2/3}]O_2$ and wet chemistry coating.

2. Experimental

2.1. Materials preparation

$Na_{2/3}[Ni_{1/3}Mn_{2/3}]O_2$ particles are synthesized through a solid state reaction. Nickel acetate ($Ni(Ac)_2 \cdot 4H_2O$) and manganese acetate ($Mn(Ac)_2 \cdot 4H_2O$) were first mixed and hand-milled in a mortar with a molar ratio of Ni:Mn=1:2. The mixture was heated up to 500 °C for 5 h with a heating rate of 3 °C/min. Sodium acetate ($NaAc \cdot 2H_2O$) was then added to the mixture with a molar ratio of Na:Ni:Mn=2.1:1:2 (5% excess sodium acetate was added in order to make up for the volatilization of Na during calcination). After that, the mixture was heated to 500 °C for 5 h again. The mixture was hand-milled once more and sintered at 950 °C for 10 h followed by annealing at 700 °C for 10 h and quenched after the annealing.

The Al_2O_3 coating was performed on the $Na_{2/3}[Ni_{1/3}Mn_{2/3}]O_2$ sample using a wet chemistry method targeting at 5 wt% of the total mass. The $Al(NO_3)_3$ salt was dissolved into deionized water with a concentration of 0.1 mol/L before a suitable amount of ammonia was added into the solution. The resulting solution was milled with $Na_{2/3}[Ni_{1/3}Mn_{2/3}]O_2$ powder and dried under stirring overnight. The mixture was annealed at 200 °C for 10 h, then sintered at 650 °C for 10 h with a heating rate of 3 °C/min and quenched after the annealing.

2.2. Materials characterization

X-ray diffraction (XRD) Bruker AMX-500 diffractometer with Cu-Kα radiation source operated at 44 kV. The surface morphology of the samples was characterized by scanning electron microscopy (SEM, JOEL JSM-7001). A field emission transmission electron microscopy (TEM, JOEL JEM 2100 F) was employed to obtain the TEM images and scanning transmission electron microscopy (STEM) images.

2.3. Electrochemical measurements

Electrodes were prepared by casting the slurry containing 85 wt% active material, 10 wt% carbon black and 5 wt% polyvinylidene fluoride (PVDF) binder onto an Al foil. The loading mass on the Al foil current collector was ~1.5 mg/cm^2.

Electrochemical tests were conducted in CR2032 coin cells with Na metal as counter electrodes and 1.2 M $NaClO_4$ in polycarbonate (PC) electrolyte with 5% fluoroethylene carbonate (FEC) by volume as additive. The stainless steel coin cell parts were coated with Al_2O_3 to prevent the side electrochemical reactions that occur at high voltage. Batteries were cycled in the voltage range of 2.5 V–4.3 V at room temperature. All capacities were calculated based on the weight of $Na_{2/3}[Ni_{1/3}Mn_{2/3}]O_2$ active material.

Electrochemical impedance spectra (EIS) and cyclic voltammetry (CV) were collected using a GAMRY Reference 600 test station. In the EIS tests, cells were tested as prepared and after charging to 4.3 V with a 10-h rest, the scan range is from 10^6 Hz to 5 mHz. In the CV tests, the scan rate is 0.01 mV/s and the scan range is from 2.5 to 4.5 V.

3. Results and discussions

In Fig. 2(a), the X-ray diffraction (XRD) pattern of the as-prepared $Na_{2/3}[Ni_{1/3}Mn_{2/3}]O_2$ powder agrees well with the P2 type $Na_{2/3}[Ni_{1/3}Mn_{2/3}]O_2$ sample (PDF 54-0894) as reported [19,28]. The XRD pattern was refined through Le Bail fitting and the d-spacing of the (002) reflection is confirmed as 5.59 angstrom accordingly. From the scanning electron microscopy (SEM) image of the as-prepared $Na_{2/3}[Ni_{1/3}Mn_{2/3}]O_2$ powder (Fig. 2(b)), the dimension of the particles varies from several micrometers to hundreds of nanometers. The energy-dispersive X-ray (EDX) mapping profiles of a single particle (Fig. 2(c)) are presented in the order of Ni (Fig. 2 (d)) and Mn (Fig. 2(e)) elements respectively. The profiles demonstrate a uniform distribution of elements in each particle and a 1:2.02 atom ratio between Ni and Mn from the EDX element spectrum in Fig. S1. From the transmission electron microscopy (TEM) image of $Na_{2/3}[Ni_{1/3}Mn_{2/3}]O_2$ particles (Fig. 2(f)), fine hexagonal crystal structures are observed, and the crystallinity of the particles is confirmed to be single crystal from the selected area

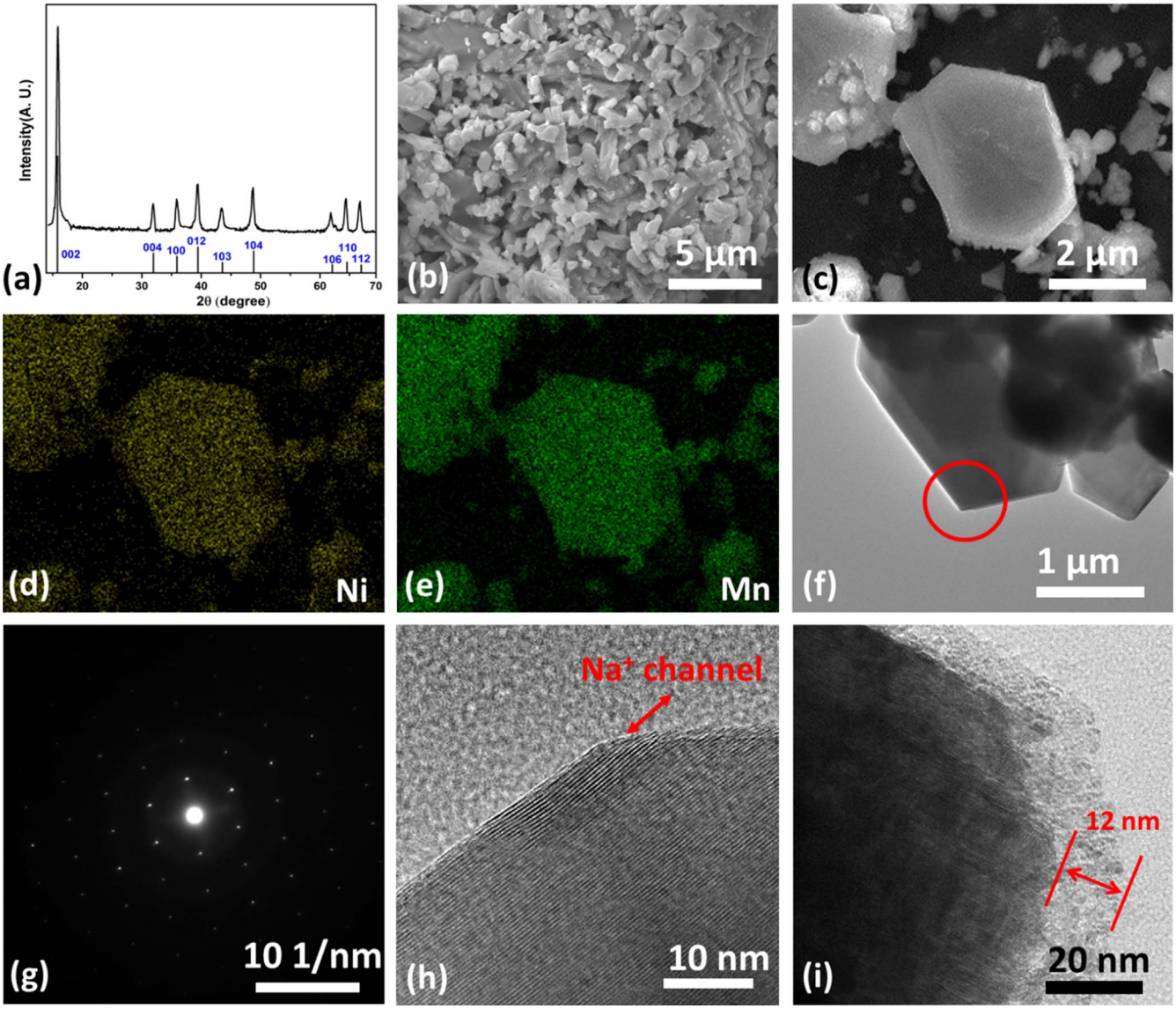

Fig. 2. (a) SEM image of as-prepared $Na_{2/3}[Ni_{1/3}Mn_{2/3}]O_2$. SEM image of a single $Na_{2/3}[Ni_{1/3}Mn_{2/3}]O_2$ particle (b), and the DEX mapping profile of elements Na (c), Ni (d) and Mn (e). (f) The TEM image of as-prepared $Na_{2/3}[Ni_{1/3}Mn_{2/3}]O_2$ and (g) the SAED pattern of the area mark in red circle in (f). The high-resolution TEM image of (h) as-prepared $Na_{2/3}[Ni_{1/3}Mn_{2/3}]O_2$ particle with Na ion channel marked and (i) Al_2O_3 coated $Na_{2/3}[Ni_{1/3}Mn_{2/3}]O_2$. (For interpretation of the references to color in this figure legend, the reader is referred to the web version of this article.)

electron diffraction (SAED) pattern presented in Fig. 2(g), where the SAED area is marked by the red circle in Fig. 2(f). The (002) lattice planes with 5.5 Å spacing are observed in the high-resolution TEM image (Fig. 2(h)), which can be confirmed as both the major ion transport channel and storage space for Na ions. The lattice parameter reaches a good agreement with the d-spacing of the (002) reflection discussed above in Fig. 2(a). For the Al_2O_3-coated sample (Al_2O_3-$Na_{2/3}Ni_{1/3}Mn_{2/3}O_2$), a ~12 nm amorphous Al_2O_3 layer was clearly observed under TEM (Fig. 2(i)). The coating is conformal both along and perpendicular to the (002) lattice plane around the particle.

The cycling performance of $Na_{2/3}[Ni_{1/3}Mn_{2/3}]O_2$ and Al_2O_3-$Na_{2/3}[Ni_{1/3}Mn_{2/3}]O_2$ cathodes was investigated by galvanostatic charge and discharge of the electrodes between 2.5 V and 4.3 V at a current density of 0.5 C rate (86.5 mA/g) as shown in Fig. 3(a). Two electrodes presents high initial specific discharge capacities around 160 mA h/g at the first sodiation process, which is close to the theoretical capacity (173 mA h/g) of P2-$Na_{2/3}[Ni_{1/3}Mn_{2/3}]O_2$. The high initial capacities of the two electrodes suggest that both samples can be fully sodiated/de-sodiated in the voltage range from 2.5 V to 4.3 V. The as-prepared $Na_{2/3}[Ni_{1/3}Mn_{2/3}]O_2$ and Al_2O_3-$Na_{2/3}[Ni_{1/3}Mn_{2/3}]O_2$ sample exhibit first charge capacities of 193 and 192 mA h/g, respectively. The extra charge capacity might involve the oxidative decomposition of sodium propyl carbonate generated at the Na metal negative electrode during the first cycle [29]. The $Na_{2/3}[Ni_{1/3}Mn_{2/3}]O_2$ cathode without any surface coating suffered from a rapidly fading capacity, retaining only 53.3% at the 50th cycles and 26.8% at the 300th cycle. This poor cycling stability is consistent with previous reports [19,21]. In contrast, the Al_2O_3-$Na_{2/3}[Ni_{1/3}Mn_{2/3}]O_2$ cathode maintains 88.4% of its initial capacity after 50 cycles, which is a visible improvement over the uncoated $Na_{2/3}[Ni_{1/3}Mn_{2/3}]O_2$ samples. At the 300th cycle, its capacity stabilized at ~115 mA h/g. Thus, the cycling stability was significantly extended by a thin layer (12 nm) Al_2O_3 coating.

For the coulombic efficiency of the two electrodes presented in Fig. 3(a), the $Na_{2/3}[Ni_{1/3}Mn_{2/3}]O_2$ cathode has an 85.3% initial efficiency that quickly rises to ~100% after the 2nd cycle. Meanwhile the Al_2O_3-$Na_{2/3}[Ni_{1/3}Mn_{2/3}]O_2$ cathode acquires 80.7% initial efficiency. Although Al_2O_3 coating is known to be able to suppress electrolyte oxidation at high voltage, here the Al_2O_3 coated sample

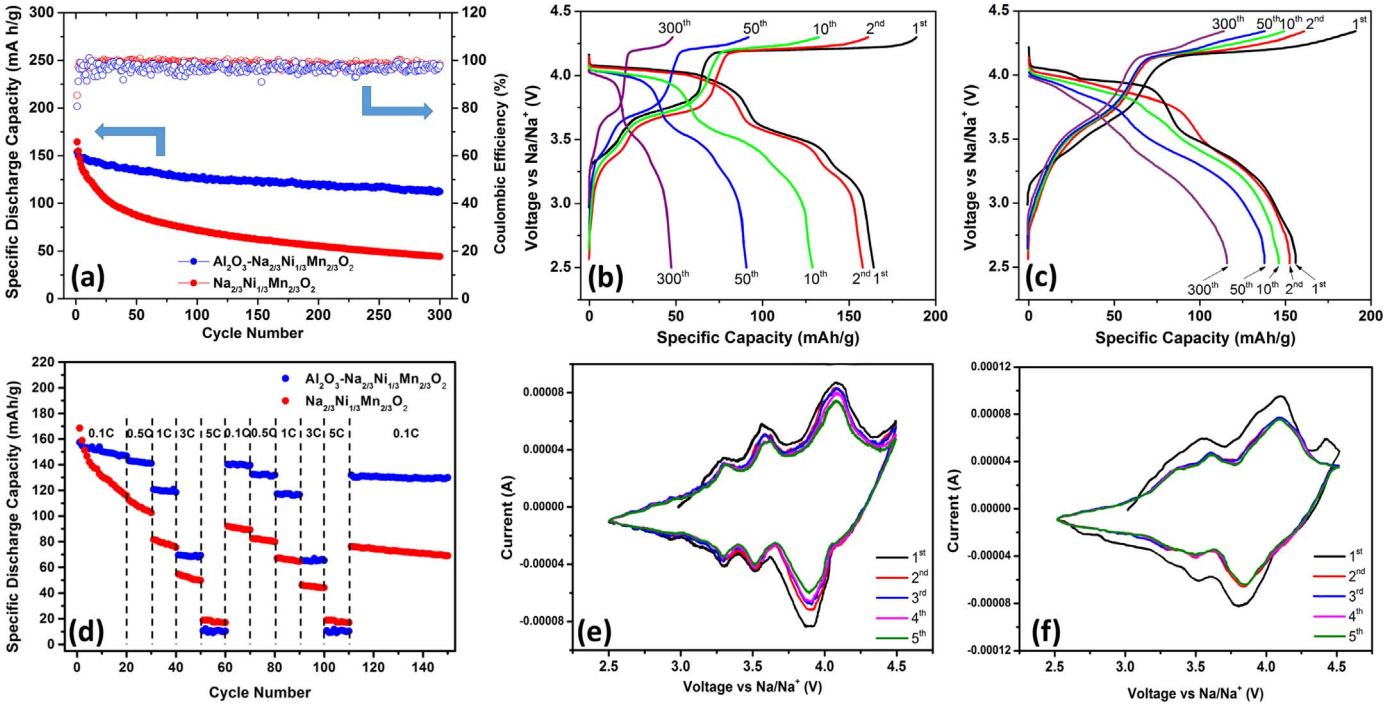

Fig. 3. (a) Cycling performance of the as-prepared $Na_{2/3}[Ni_{1/3}Mn_{2/3}]O_2$ and Al_2O_3-$Na_{2/3}[Ni_{1/3}Mn_{2/3}]O_2$. The charge and discharge profiles of (b) $Na_{2/3}[Ni_{1/3}Mn_{2/3}]O_2$ electrodes and (c) Al_2O_3-$Na_{2/3}[Ni_{1/3}Mn_{2/3}]O_2$ electrode. (d) Rate performance of the as-prepared $Na_{2/3}[Ni_{1/3}Mn_{2/3}]O_2$ and Al_2O_3-$Na_{2/3}[Ni_{1/3}Mn_{2/3}]O_2$. Cyclic voltammetry profiles of (e) as-prepared $Na_{2/3}[Ni_{1/3}Mn_{2/3}]O_2$ cathode and (f)Al_2O_3-$Na_{2/3}[Ni_{1/3}Mn_{2/3}]O_2$ cathode.

shows a slightly lower initial coulombic efficiency. This may be due to the Al_2O_3 coating layer further increases the kinetic battier for extraction of Na ions out of the metal oxide component. The slightly lower efficiency of the Al_2O_3-$Na_{2/3}[Ni_{1/3}Mn_{2/3}]O_2$ cathode in the following cycles may be related to the low electronic conductivity of the Al_2O_3 coating.

Aside from capacity, voltage profiles actually reveal additional details about the electrochemical sodiation/de-sodiation process in these cathode materials. The voltage profiles of the $Na_{2/3}[Ni_{1/3}Mn_{2/3}]O_2$ and Al_2O_3-$Na_{2/3}[Ni_{1/3}Mn_{2/3}]O_2$ cathodes are depicted in Fig. 3(b) and (c) respectively, with cycle numbers labeled on individual curves. The uncoated $Na_{2/3}[Ni_{1/3}Mn_{2/3}]O_2$ sample shows three potential plateaus at 3.3–3.4, 3.7 and 4.2 V in its first de-sodiation process corresponding to the Na content of 2/3, 1/2 and 1/3, respectively. On the other hand, the Al_2O_3-$Na_{2/3}[Ni_{1/3}Mn_{2/3}]O_2$ shows a slope from 3.3 to 3.7 V and a plateau at 4.2 V. For the charge curves of the 2nd, 10th, 50th and 300th cycle, all plateaus of the uncoated $Na_{2/3}[Ni_{1/3}Mn_{2/3}]O_2$ decay rapidly with increasing cycle number. However, for the Al_2O_3-$Na_{2/3}[Ni_{1/3}Mn_{2/3}]O_2$ cathode, the charge capacity decay mainly happens on the high potential plateau at 4.2 V, which implies the P2-O2 phase transition only occurs in the region of $0 \leq x \leq 1/3$ for the $Na_{2/3-x}[Ni_{1/3}Mn_{2/3}]O_2$ cathode [28]. For all discharge curves of both samples, two major potential plateaus at 4.1 and 3.7 V were observed for both cathodes. However, in contrast to the uncoated $Na_{2/3}[Ni_{1/3}Mn_{2/3}]O_2$, the discharge plateaus of the Al_2O_3-$Na_{2/3}[Ni_{1/3}Mn_{2/3}]O_2$ evolve to slopes, which indicates that the Na ion transition in the Al_2O_3-$Na_{2/3}[Ni_{1/3}Mn_{2/3}]O_2$ is more inclined to a solid solution diffusion mode. Similar to the charge curves, the discharge plateaus of the uncoated $Na_{2/3}[Ni_{1/3}Mn_{2/3}]O_2$ were shortened as the cycle number increased, but the Al_2O_3-$Na_{2/3}[Ni_{1/3}Mn_{2/3}]O_2$ showed a much smaller capacity decay owing to the Al_2O_3 surface coating.

In the rate capability test (Fig. 3(d)), the capacities of the two electrodes decay in the first 60 cycles from 0.1 C to 5 C charge/discharge rate. The uncoated $Na_{2/3}[Ni_{1/3}Mn_{2/3}]O_2$ sample shows a larger fading rate than the Al_2O_3-$Na_{2/3}[Ni_{1/3}Mn_{2/3}]O_2$ sample, which reaches a good agreement with the cycling performance presented in Fig. 3(a). However, the capacity of the Al_2O_3-$Na_{2/3}[Ni_{1/3}Mn_{2/3}]O_2$ was stabilized after 60 cycles, and the cathode can deliver average capacities of 140.2, 132.4, 116.9, and 65.3 mA h/g at 0.1, 0.5, 1 and 3 C rate. At 5 C charge/discharge rate, the capacity of the Al_2O_3 coated sample decays to almost zero; on the other hand, the uncoated $Na_{2/3}[Ni_{1/3}Mn_{2/3}]O_2$ cathode can deliver around 20 mA h/g capacity, which suggests that the Al_2O_3 coating increases the electronic resistance and further enlarges the polarization of the material. The capacity of the Al_2O_3-$Na_{2/3}[Ni_{1/3}Mn_{2/3}]O_2$ was stabilized at $\sim$130 mA h/g at 0.1 C after 110 cycles, meanwhile the capacity of the uncoated $Na_{2/3}[Ni_{1/3}Mn_{2/3}]O_2$ sample continued to decay.

To understand the role of the Al_2O_3 surface coating during Na-ion transport, electrochemical impedance spectra (EIS) were obtained to analyze and compare the reaction resistances of the two electrodes. EIS tests were performed on fresh cells and cells first charged to 4.3 V with a 10-h rest. The Nyquist plots of the cells under different conditions are shown in Fig. S2a and b respectively with enlarged high frequency regions inserted. In Fig. S2a, for the fresh $Na_{2/3}[Ni_{1/3}Mn_{2/3}]O_2$/Na cell, the impedance spectra is typically composed of one semicircle in the high frequency region and a straight slopping line at low frequencies, corresponding to the Na ion charge transfer impedance and diffusion resistance. Compared to the uncoated $Na_{2/3}[Ni_{1/3}Mn_{2/3}]O_2$/Na fresh cell, the impedance spectra of Al_2O_3-$Na_{2/3}[Ni_{1/3}Mn_{2/3}]O_2$ fresh cell shows another semicircle at medium-frequencies between the first semicircle and the diffusion sloping line, which could be attributed to the charge transfer impedance of the Al_2O_3 layer coated on $Na_{2/3}[Ni_{1/3}Mn_{2/3}]O_2$ particles. Moreover, in the high frequency region inserted in Fig. S2a, the Al_2O_3-$Na_{2/3}[Ni_{1/3}Mn_{2/3}]O_2$ presents a slightly larger impedance at the intersection point between the spectra and Z_{Re} axis, which corresponds to a larger contact resistance. In Fig. S2b, for cells firstly charged to 4.3 V, both of the cells show Nyquist plots containing a semicircle and a diffusion tail, but with smaller contact and charge transfer resistance

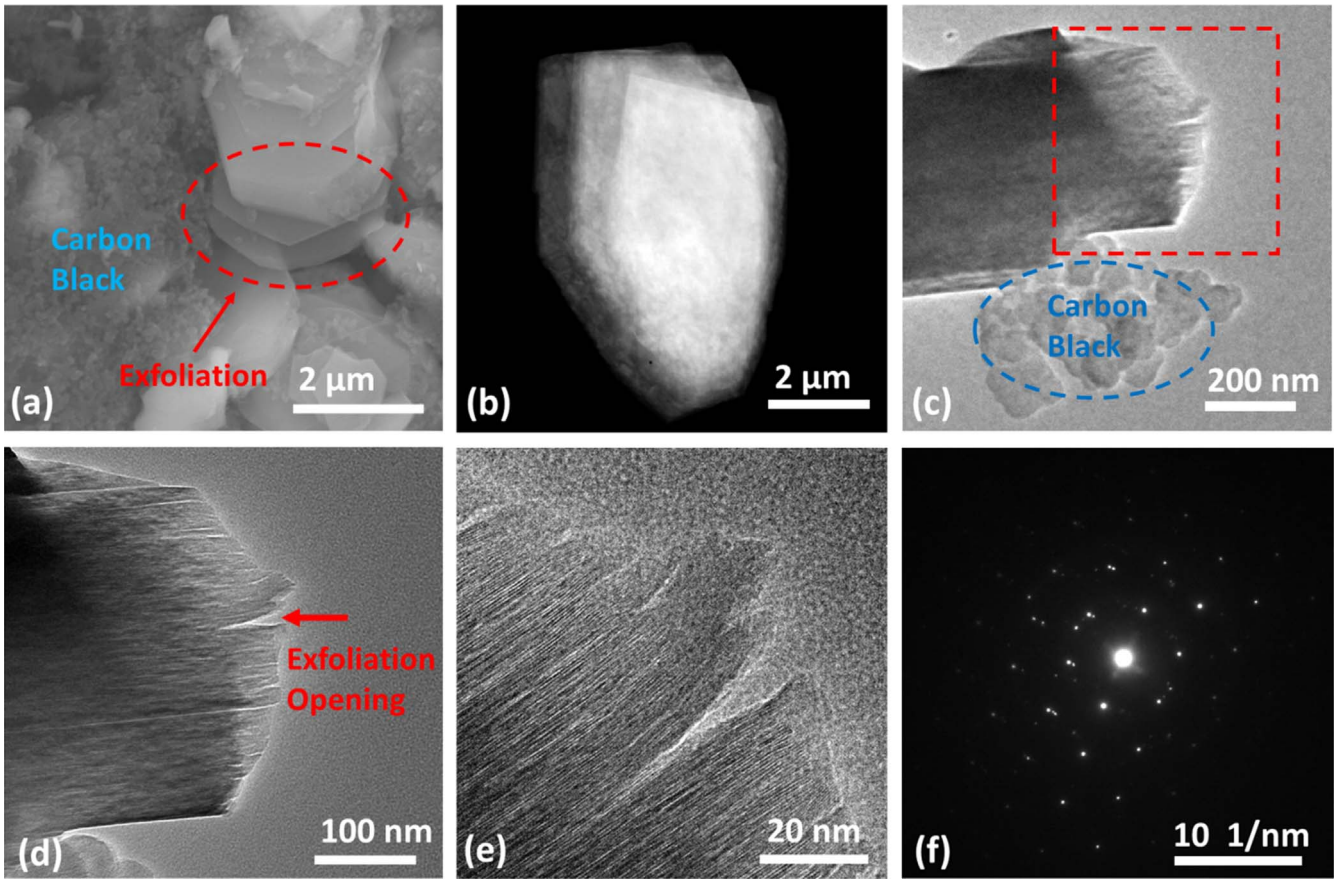

Fig. 4. (a) SEM image of after-cycling $Na_{2/3}[Ni_{1/3}Mn_{2/3}]O_2$ electrode with the exfoliation and carbon black areas marked. (b) STEM of an after-cycling $Na_{2/3}[Ni_{1/3}Mn_{2/3}]O_2$ particle. (c) TEM image of an after-cycling $Na_{2/3}[Ni_{1/3}Mn_{2/3}]O_2$ particle. (d) Enlarged TEM image of the area marked in (c). (e) High-resolution TEM image of the exfoliation opening in (d). (f) The SAED pattern of the area marked in (c).

compared to the as-prepared cells.

The sodiation and de-sodiation processes of as-prepared $Na_{2/3}[Ni_{1/3}Mn_{2/3}]O_2$ and Al_2O_3-$Na_{2/3}[Ni_{1/3}Mn_{2/3}]O_2$ cathodes were also characterized using cyclic voltammetry (CV), as shown in Fig. 4 (e) and (f). For the uncoated $Na_{2/3}[Ni_{1/3}Mn_{2/3}]O_2$ sample, four peaks at 3.3, 3.6, 4.1 and 4.5 V were observed in the first and subsequent de-sodiation processes. The peak at 4.5 V in the de-sodiation curves can be mainly assigned to the side reactions at high voltage such as electrolyte decomposition and surface corrosion of the material [30]. One sharp peak at 3.9 V with fast decay and another two peak at 3.3 and 3.5 V were observed in the subsequent sodiation processes. In Fig. 4(f), the Al_2O_3-$Na_{2/3}[Ni_{1/3}Mn_{2/3}]O_2$ sample shows a very different curve for the first de-sodiation process with three peaks located at 3.6 and 4.1 V, indicating a different SEI formation mechanism on the Al_2O_3 surface [31]. Compared to the uncoated $Na_{2/3}[Ni_{1/3}Mn_{2/3}]O_2$ sample, Al_2O_3-$Na_{2/3}[Ni_{1/3}Mn_{2/3}]O_2$ shows similar peak positions in the following cycles but with broader peak features except the peaks at 3.3 V, which becomes to a small shoulder. The peak at 4.4 V was suppressed for the Al_2O_3-$Na_{2/3}[Ni_{1/3}Mn_{2/3}]O_2$ sample, indicating that the Al_2O_3 coating can effectively mitigate side reactions at high voltage.

To gain insight into the capacity fading mechanism of $Na_{2/3}[Ni_{1/3}Mn_{2/3}]O_2$, SEM and TEM images were collected after 300 cycles. In the after-cycling SEM image of the uncoated $Na_{2/3}[Ni_{1/3}Mn_{2/3}]O_2$ electrode shown in Fig. 4(a) and Fig. S3, several semitransparent layers with clear hexagonal shape were observed, which were identified as the exfoliated layers from the $Na_{2/3}[Ni_{1/3}Mn_{2/3}]O_2$ single particle. This exfoliation phenomenon can also be confirmed from the after-cycling scanning transmission electron microscope (STEM) image in Fig. 4(b), which shows one $Na_{2/3}[Ni_{1/3}Mn_{2/3}]O_2$ single crystal particle exfoliated into 3 pieces. More details about the exfoliation can be found in the after-cycling TEM image of the $Na_{2/3}[Ni_{1/3}Mn_{2/3}]O_2$. In Fig. 4(c) and its enlarged view (Fig. 4(d)), a very obvious exfoliation opening can be clearly observed. Furthermore, in the high-resolution TEM image (Fig. 4(e)), the exfoliation opening can be defined to be along the (002) plane direction, which is the Na ion storage space and also the major transfer channel described in Fig. 2(h).

The exfoliation phenomena observed above also agrees well with the changes in the XRD pattern of the after-cycling $Na_{2/3}[Ni_{1/3}Mn_{2/3}]O_2$ electrode: in Fig. 5(b) and its enlarged view from 15° to 17° (Fig. 5(a)), the (002) lattice peak shows an obvious shift to the left from 15.8° to 15.3°, suggesting the (002) lattice space was expanded during cycling, and further proves that exfoliation should be a consequence of the lattice space expansion. Compared to the single crystal SAED pattern of the as-prepared sample, the SAED pattern of the after-cycling $Na_{2/3}[Ni_{1/3}Mn_{2/3}]O_2$ indicates a phase transition during cycling within the high voltage window, which may be due to the introduction of the O2 stacks [19]. Part of this crystal structure change can also be detected from the XRD pattern of the after-cycling $Na_{2/3}[Ni_{1/3}Mn_{2/3}]O_2$ electrode in Fig. 5 (a) and (b) where almost all peaks show phase separation besides the shifted (002) peak. This implies that the phase separation occurs during cycling and part of this transition is irreversible and harmful to the crystal structure stability. Since the P2-O2 transformation requires no bond breaking between oxygen and transition metal, and also considering the O2 phase has a larger

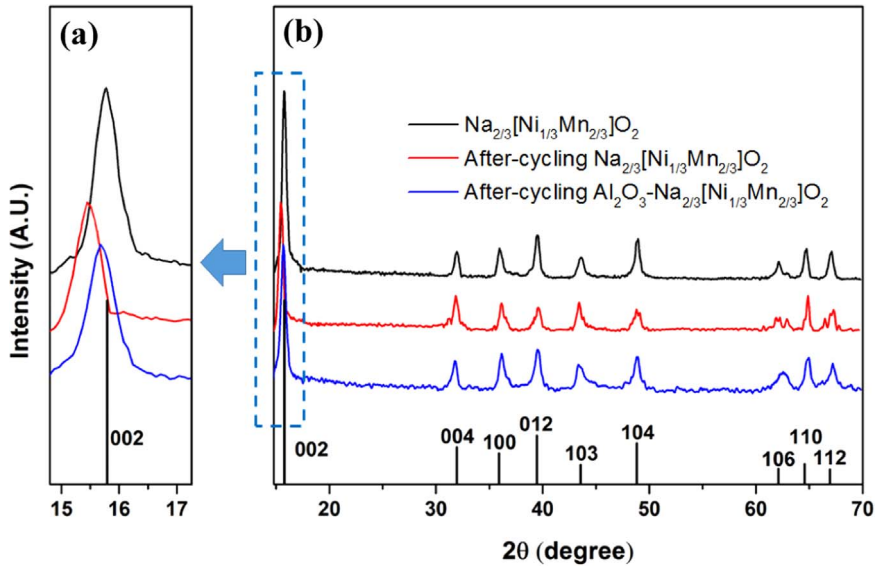

Fig. 5. The XRD pattern of the as-prepared $Na_{2/3}[Ni_{1/3}Mn_{2/3}]O_2$, after-cycling $Na_{2/3}[Ni_{1/3}Mn_{2/3}]O_2$ and after-cycling Al_2O_3-$Na_{2/3}[Ni_{1/3}Mn_{2/3}]O_2$. (a) is the enlarged view of (b) from 15° to 17°.

volume change (more than 20%) than the P2 phase during sodiation/de-sodiation, it is reasonable to believe that the exfoliation occurred during the Na-ion intercalation in the high voltage region. Besides the insertion and extraction of Na ions, the exfoliation also possibly involves side reactions such as surface oxidation at high voltage, since the exfoliation was observed starting from the surface of the bulk material. Once the exfoliation happens, the P2-O2 phase transition loop will be broken permanently and part of the Na ion storage space will be eliminated. The exfoliation is definitely harmful for a cathode material that aims for stable electrochemical performance.

In hope of investigating how the Al_2O_3 coating can improve the cycling stability of the cathode material, SEM and TEM images with the SAED pattern of the after-cycling Al_2O_3-$Na_{2/3}[Ni_{1/3}Mn_{2/3}]O_2$ electrode are also collected. In the SEM image of after-cycling Al_2O_3-$Na_{2/3}[Ni_{1/3}Mn_{2/3}]O_2$ electrode (Fig. 6(a)), several active material particles are embedded in the electrode without any sign of exfoliation. In the high-resolution TEM image of the after-cycling Al_2O_3-$Na_{2/3}[Ni_{1/3}Mn_{2/3}]O_2$ (Fig. 6(b)), part of the Al_2O_3 coating is peeled off from the particles, which may be due to the large volume change of the O2 phase during Na ion storage and release. However, no exfoliation opening was found in the TEM image, which proved that the Al_2O_3 coating efficiently protected the $Na_{2/3}[Ni_{1/3}Mn_{2/3}]O_2$ crystal structure by suppressing the exfoliation. From the SAED pattern in Fig. 6(c), only a slight phase transition is detected for the after-cycling Al_2O_3-$Na_{2/3}[Ni_{1/3}Mn_{2/3}]O_2$ compared to the uncoated sample. The morphology difference between the after-cycling samples with and without surface coating can also be observed from their XRD patterns. In Fig. 5(a), the shift of the (002) peak is only ~0.1° for the after-cycling Al_2O_3-$Na_{2/3}[Ni_{1/3}Mn_{2/3}]O_2$ compared to the as-prepared $Na_{2/3}[Ni_{1/3}Mn_{2/3}]O_2$, which is much smaller than the shift of the after-cycling $Na_{2/3}[Ni_{1/3}Mn_{2/3}]O_2$ without surface coating (~0.5°). In Fig. 5(b), no obvious peak separation was detected from the XRD pattern of the after-cycling Al_2O_3-$Na_{2/3}[Ni_{1/3}Mn_{2/3}]O_2$ sample. The difference of the XRD data of those two after-cycling samples suggests that the Al_2O_3 surface coating can efficiently suppress the phase separation and avoid the crystal structure damage introduced by the phase transition during long-term cycling.

In order to exam whether Mn element reduction and dissolution at high potential is part of the reason for the capacity fading, we also collected the EDX data from the dried Na metal counter

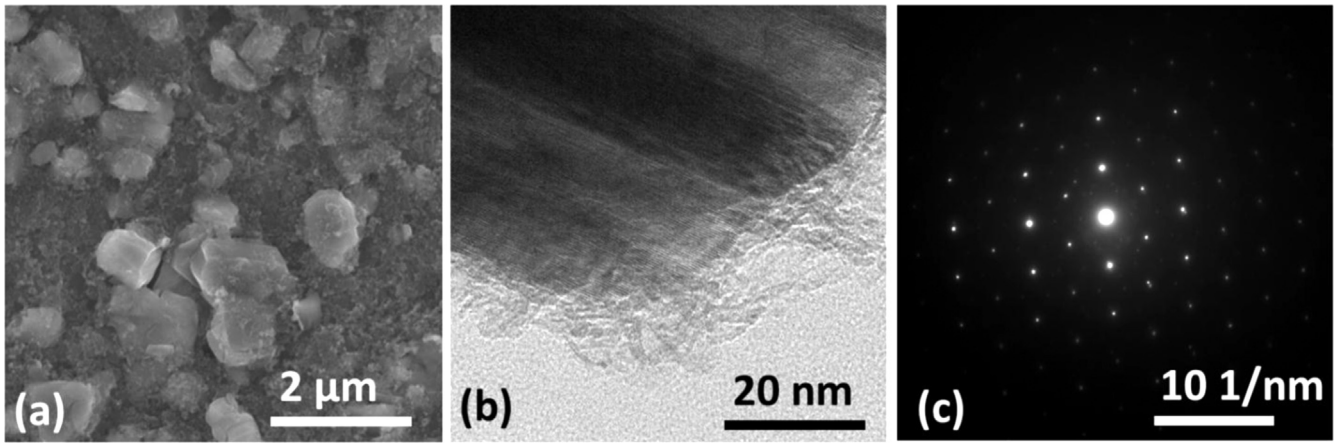

Fig. 6. (a) The SEM image of the after-cycling Al_2O_3-$Na_{2/3}[Ni_{1/3}Mn_{2/3}]O_2$ electrode. (b) The high-resolution TEM image of an after-cycling Al_2O_3-$Na_{2/3}[Ni_{1/3}Mn_{2/3}]O_2$ particle. (c) The SAED pattern of the after-cycling Al_2O_3-$Na_{2/3}[Ni_{1/3}Mn_{2/3}]O_2$ particle.

electrode and the surface of the separator facing to the Na metal from the after-cycling cells without any washing. However, from the EDX point element analysis in several locations (Fig. S4), no Mn element signals were detected. This result suggests that Mn dissolution is not the main reason that leads to the capacity decay in our case.

Our results demonstrate that the exfoliation of the $Na_{2/3}[Ni_{1/3}Mn_{2/3}]O_2$ involves both a crystal phase transition and volume expansion of the O2 phase. Thus, we believe that external mechanical support is necessary in order to stabilize the crystal structure and enhance the electrochemical performance. The above experimental data revealed that the Al_2O_3 coating prevents the mechanical degradation of $Na_{2/3}[Ni_{1/3}Mn_{2/3}]O_2$ and also explains the electrochemical cycling stability improvement of the Al_2O_3-$Na_{2/3}[Ni_{1/3}Mn_{2/3}]O_2$ sample. It is clear that the Al_2O_3 surface coating cannot only reduce the side reaction at high voltage, but can also give mechanical support to help the bulk material to maintain its layered structure, which can increase the reversibility of the P2-O2-P2 phase transition loop during charge/discharge process. This Al_2O_3 surface coating unlocks the stable cycling performance of P2-$Na_{2/3}[Ni_{1/3}Mn_{2/3}]O_2$ within high voltage window and releases the high energy density of this layered structure cathode material for Na-ion batteries. Other surface coating methods or scaffold matrices may also improve the performance of the layered structure cathode for Na-ion batteries based on the exfoliation induced decay mechanism discovered in this paper and will be studied in the future.

4. Conclusions

In summary, we first investigated the capacity decay mechanism of the layered structure P2-$Na_{2/3}[Ni_{1/3}Mn_{2/3}]O_2$, and the exfoliation phenomena associated with the phase transition was analyzed. Furthermore, the cycling stability of the $Na_{2/3}[Ni_{1/3}Mn_{2/3}]O_2$ cathode in the high voltage range was significantly enhanced and the exfoliation was efficiently suppressed by a thin layer of Al_2O_3 surface coating, which demonstrated that the Al_2O_3 coating can provide superior protection to this P2 type layered structure material. The stable high voltage Al_2O_3-$Na_{2/3}[Ni_{1/3}Mn_{2/3}]O_2$ represents a new strategy for the development of inexpensive and high power/energy Na-based energy storage applications.

Acknowledgment

We would like to acknowledge the collaboration of this research with King Abdul-Aziz City for Science and Technology (KACST) via The Center of Excellence for Nanotechnologies (CEGN). We acknowledge the funding support from the University of Southern California. A portion of the images and data used in this article were acquired at The Center for Electron Microscopy and Microanalysis, University of Southern California.

Appendix A. Supplementary material

Supplementary data associated with this article can be found in the online version at http://dx.doi.org/10.1016/j.nanoen.2016.06.026.

References

[1] P.G. Bruce, B. Scrosati, J.-M. Tarascon, Angew. Chem. Int. Ed. 47 (2008) 2930–2946.
[2] W. Luo, F. Shen, C. Bommier, H. Zhu, X. Ji, L. Hu, Acc. Chem. Res. 49 (2016) 231–240.
[3] B.L. Ellis, W.R.M. Makahnouk, Y. Makimura, K. Toghill, L.F. Nazar, Nat. Mater. 6 (2007) 749–753.
[4] Y. Zhu, Y. Xu, Y. Liu, C. Luo, C. Wang, Nanoscale 5 (2013) 780–787.
[5] A. Langrock, Y. Xu, Y. Liu, S. Ehrman, A. Manivannan, C. Wang, J. Power Sources 223 (2013) 62–67.
[6] Y. Liu, Y. Xu, X. Han, C. Pellegrinelli, Y. Zhu, H. Zhu, J. Wan, A.C. Chung, O. Vaaland, C. Wang, L. Hu, Nano Lett. 12 (2012) 5664–5668.
[7] Y. Lu, L. Wang, J.B. Goodenough, Chem. Commun. 48 (2012) 6544–6546.
[8] C.D. Wessells, S.V. Peddada, R.A. Huggins, Y. Cui, Nat. Commun. 2 (2011) 5421–5425.
[9] X. Xia, J.R. Dahn, Electrochem. Solid-State Lett. 15 (2012) A1–A4.
[10] D. Kundu, E. Talaie, V. Duffort, L.F. Nazar, Angew. Chem. Int. Ed. 54 (2015) 3431–3448.
[11] S. Xu, Y. Wang, L. Ben, Y. Lyu, N. Song, Z. Yang, Y. Li, Y. Mu, H. –T. Yang, L. Gu, Y.–S. Hu, H. Li, Z.–H. Cheng, L. Chen, X. Huang, Adv. Energy Mater. (2015), http://dx.doi.org/10.1002/aenm. 201501156.
[12] L. Liu, X. Li, S.–H. Bo, Y. Wang, H. Chen, N. Twu, D. Wu, G. Ceder, Adv. Energy Mater. (2015), http://dx.doi.org/10.1002/aenm. 201500944.
[13] G. Yuan, X. Hu, J. Qian, F. Pei, F. Wu, R. Mao, R. Ai, H. Yang, Y. Cao, Electrochim. Acta 116 (2014) 300–305.
[14] N. Yabuuchi, M. Kajiyama, J. Iwatate, H. Nishikawa, S. Hitomi, R. Okuyama, R. Usui, Y. Yamada, S. Komaba, Nat. Mater. 11 (2012) 512–517.
[15] S. Komaba, N. Yabuuchi, T. Nakayama, A. Ogata, T. Ishikawa, I. Nakai, Inorg. Chem. 51 (2012) 6211–6220.
[16] X. Ma, H. Chen, G. Ceder, J. Electrochem. Soc. 158 (2011) A1307–A1312.
[17] Q. Zhong, A. Bonakdarpour, M. Zhang, Y. Gao, J.R. Dahn, J. Electrochem. Soc. 114 (1997) A205–A213.
[18] X. Fang, C. Shen, M. Ge, J. Rong, Y. Liu, A. Zhang, F. Wei, C. Zhou, Nano Energy 12 (2015) 43–51.
[19] Z. Lu, J.R. Dahn, J. Electrochem. Soc. 148 (2011) A1225–A1229.
[20] M.H. Han, E. Gonzalo, E. Singh, T. Rojo, Energy Environ. Sci. 8 (2015) 81–102.
[21] H. Yoshida, N. Yabuuchi, K. Kubota, I. Ikeuchi, A. Garsuch, M. Schulz-Dobrick, S. Komaba, Chem. Commun. 50 (2014) 3677–3680.
[22] D. Kim, E. Lee, M. Slater, W. Lu, S. Rood, C.S. Johnson, Electrochem. Commun. 18 (2012) 66–69.
[23] Y. He, Y. Yu, Y. Wang, H. Li, X. Huang, Adv. Mater. 23 (2011) 4938–4941.
[24] X. Xiao, P. Lu, D. Ahn, Adv. Mater. 23 (2011) 3911–3915.
[25] H. Zhu, Z. Jia, Y. Chen, N. Weadock, J. Wan, O. Vaaland, X. Han, T. Li, L. Hu, Nano Lett. 13 (2013) 3093–3100.
[26] Y. Liu, X. Fang, M. Ge, J. Rong, C. Shen, A. Zhang, H.A. Enaya, C. Zhou, Nano Energy 16 (2015) 399–407.
[27] Z. Lu, J.R. Dahn, Chem. Mater. 13 (2001) 1252–1257.
[28] D.H. Lee, J. Xu, Y.S. Meng, Phys. Chem. Chem. Phys. 15 (2013) 3304–3312.
[29] S. Komaba, T. Ishikawa, N. Yabuuchi, W. Murata, A. Ito, Y. Ohsawa, ACS Appl. Mater. Interfaces 3 (2011) 4165–4168.
[30] P. Yan, A. Nie, J. Zheng, Y. Zhou, D. Lu, X. Zhang, R. Xu, I. Belharouak, X. Zu, J. Xiao, K. Amine, J. Liu, F. Gao, R. Shahbazian-Yassar, J.G. Zhang, C.M. Wang, Nano Lett. 15 (2015) 514–522.
[31] P. Yan, J. Zheng, X. Zhang, R. Xu, K. Amine, J. Xiao, J. –G. Zhang, C. –M. Wang, Chem. Mater. (2015), http://dx.doi.org/10.1021/acs.ChemMater.5b04301.

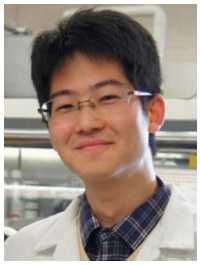

Yihang Liu is currently pursuing his Ph.D. under the supervision of Prof. Chongwu Zhou in Ming Hsieh Department of Electrical Engineering at University of Southern California. He received a master degree in Chemical Engineering from University of Maryland, College Park and a bachelor degree in Opto-Electronic Engineering from Beijing Institute of Technology, China. His research interests are energy storage devices, including Li-ion and Na-ion batteries.

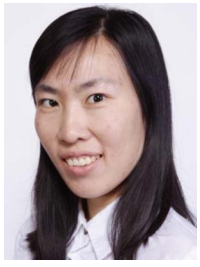

Xin Fang received her Bachelor's degree from University of Science and Technology of China in 2010. She is currently pursuing her Ph.D. under the supervision of Prof. Chongwu Zhou in Mork Family Department of Chemical Engineering and Materials Science, University of Southern California. Her research mainly focuses on synthesis and modification of materials for energy storage and semiconductor devices.

Anyi Zhang received his Bachelor's degree from the Department Chemical Engineering at Zhejiang University in 2011 and Master's degree from the Mork Family Department of Chemical Engineering and Materials Science at University of Southern California in 2013. He is currently pursuing his Ph.D. under the supervision of Prof. Chongwu Zhou at Mark Family Department of Chemical Engineering and Materials Science, University of Southern California. His research interests mainly focus on lithium-sulfur Batteries.

Chenfei Shen received his Bachelor's degree from Department of Materials Science at Nanjing University of Aeronautics and Astronautics in 2011 and Master's degree from University of California, Los Angeles in 2012. He is currently pursuing his Ph.D. under the supervision of Prof. Chongwu Zhou at Mork Family Department of Chemical Engineering and Materials Science, University of Southern California. His research interests mainly focus on energy storage devices.

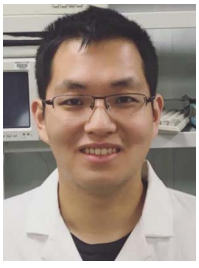

Qingzhou Liu is currently pursuing his Ph.D. under the supervision of Prof. Chongwu Zhou in Department of Material Science at University of Southern California. He received a master degree in Chemical Engineering from University of Southern California and a bachelor degree in Chemistry from University of Science and Technology of China. His research interests are nano-electronics and bio-nano sensors.

Dr. Enaya is currently an Assistant Research Professor in The Center of Excellence for Green Nanotechnologies at KACST and UCLA. His current research focuses on high frequency nano devices, nano-enabled energy storage, and spintronics. Dr. Enaya is also a co-founder of Carbonics, a startup that provides RF semiconductor solutions to cope with the higher frequency and tough linear requirements for next generation wireless products. Dr. Enaya received his B. S. and Ph.D. in Electrical Engineering from North Carolina State University, where he joined Dr. Ki Wook Kim group to investigate nonvolatile spin memory devices based on diluted magnetic semiconductors.

Dr. Chongwu Zhou is a full professor of Department of Electrical Engineering at University of Southern California (USC). He previously held positions of Jack Munushian Associate Professor (2006–2011) and Assistant Professor (2000–2006) at USC. He received Bachelor's Degree from the University of Science and Technology of China in 1993, received Ph.D. in Electrical Engineering from Yale University in 1999, and worked as a postdoc at Stanford University from 1998 to 2000. His research interest covers nanomaterials, nanoelectronics, energy nanotechnology, and bionanotechnology. He is an Associate Editor for Nanotechnology and IEEE Transactions on Nanotechnology, and serves as an Editorial Advisory Board member for ACS Nano.